Radioimaging of Light Chain Amyloid with a Fibril-Reactive Monoclonal Antibody

Jonathan S. Wall[1], Stephen J. Kennel[1], Mike Paulus[2], Jens Gregor[3], Tina Richey[1], James Avenell[4], Jeffrey Yap[4], David Townsend[4], Deborah T. Weiss[1], and Alan Solomon[1]

[1]Human Immunology and Cancer Program, Department of Medicine, University of Tennessee Graduate School of Medicine, Knoxville, Tennessee; [2]Engineering Science and Technology Group, Oak Ridge National Laboratory, Oak Ridge, Tennessee; [3]Department of Computer Science, University of Tennessee, Knoxville, Tennessee; and [4]Cancer Imaging and Tracer Development Research Program, University of Tennessee Graduate School of Medicine, Knoxville, Tennessee

Currently, there are no available means in the United States to document objectively the location and extent of amyloid deposits in patients with systemic forms of amyloidosis. To address this limitation, we have developed a novel diagnostic strategy, namely, the use of a radiolabeled fibril-reactive murine monoclonal antibody (mAb) as an amyloid-specific imaging agent. The goal of this study was to determine the pharmacokinetics, biodistribution, and ability of this reagent to target the type of amyloid that is formed from immunoglobulin light chains, that is, AL. **Methods:** Subcutaneous tumors (amyloidomas) were induced in BALB/c mice by injection of human AL fibrils. The IgG1 mAb designated 11-1F4 and an isotype-matched control antibody were radioiodinated, and the pharmacokinetics and localization of these reagents were determined from blood and tissue samples. Amyloidoma-bearing animals that received ^{125}I- or ^{124}I-labeled antibodies were imaged by whole-body small-animal SPECT/CT or small-animal PET/CT technology, respectively. **Results:** Radioiodinated mAb 11-1F4 retained immunoreactivity, as evidenced by its subnanomolar affinity for light chains immobilized on 96-well microtiter plates and for beads conjugated with a light chain–related peptide. Additionally, after intravenous administration, the labeled reagents had the expected biologic half-life of murine IgG1, with monoexponential whole-body clearance kinetics. In the amyloidoma mouse model, ^{125}I-11-1F4 was predominately localized in the tumors, as demonstrated in biodistribution and autoradiographic analyses. The mean uptake of this reagent, that is, the percentage injected dose per gram of tissue, 72 h after injection was significantly higher for amyloid than for skeletal muscle, spleen, kidney, heart, liver, or other tissue samples. Notably, the accumulation within the amyloidomas of ^{125}I- or ^{124}I-11-1F4 was readily visible in the fused small-animal SPECT/CT or small-animal PET/CT images, respectively. **Conclusion:** Our studies demonstrate the amyloid-imaging capability of a radiolabeled fibril-reactive mAb and provide the basis for a clinical trial designed to determine its diagnostic potential in patients with AL amyloidosis and other systemic amyloidoses.

Received Jun. 29, 2006; revision accepted Sep. 19, 2006.

For correspondence or reprints contact: Jonathan S. Wall, PhD, University of Tennessee Graduate School of Medicine, 1924 Alcoa Hwy., Knoxville, TN 37920.

E-mail: jwall@mc.utmck.edu

Key Words: amyloid; immunoimaging; small-animal SPECT/CT; small-animal PET/CT

J Nucl Med 2006; 47:2016–2024

The ability to image a pathologic process radiographically provides physicians with an objective means to determine the presence and extent of disease as well as to monitor a patient's response to treatment or determine whether relapse has occurred. For the systemic amyloidoses, routine radiologic techniques (e.g., CT, ultrasound, or MRI) are not particularly informative or amyloid specific. For primary (light chain amyloid [AL]) or secondary (amyloid A [AA]) amyloidosis, European investigators have successfully imaged pathologic deposits by planar scintigraphy with ^{123}I-labeled P component and with ^{99m}Tc-aprotinin (*1–4*); however, the U.S. Food and Drug Administration will not permit the administration of such reagents in the United States inasmuch as the protein carriers are of human and animal origins, respectively.

Given this restriction and the need to document the presence of amyloid fibrils in affected major organs quantitatively, especially in patients enrolled in therapeutic clinical trials, we have proposed another strategy, namely, the use of a radiolabeled fibril-reactive monoclonal antibody (mAb) as an imaging agent. The rationale for this approach is based on the discovery that certain murine anti–human light chain mAbs recognize a conformational epitope common to fibrils formed from light chains as well as other amyloidogenic precursor molecules, such as serum AA, transthyretin, and apolipoprotein A-I (*5*). Further, when the prototypic IgG1 antibody designated 11-1F4 was administered to mice bearing subcutaneous human AL amyloidomas, it bound specifically to the amyloid deposits and accelerated the removal of this material.

On the basis of these data, we have tested whether mAb 11-1F4 labeled with γ- or positron-emitting isotopes of iodine would prove to be a suitable reagent for the visualization of amyloid. For these studies, we used instrumentation

designed to image small laboratory animals, that is, high-resolution small-animal SPECT and small-animal PET co-registered with small-animal CT for anatomic precision. We now report our experimental findings, which indicated the feasibility of immunoimaging as a clinical means to document the presence and distribution of systemic amyloid deposits.

MATERIALS AND METHODS

Amyloid Proteins

Amyloid fibrils were extracted (*6*) from livers or spleens obtained postmortem from patients with AL amyloidosis, and their chemical compositions were determined by amino acid sequencing and tandem mass spectrometry (*7*). Synthetic amyloid fibrils were prepared (*8*) from a synthetic peptide (Keck Biotechnology Center) that encompassed the first 30 residues of human κ4 light chain Len (Len 1–30) (*9*), which was used as the immunogen to generate mAb 11-1F4 (*10*).

Antibodies

The derivation as well as the production of amyloid-reactive murine IgG1 mAb 11-1F4 by the National Cancer Institute Biopharmaceutical Development Program (Science Applications International Corporation) was previously reported (*11,12*). An isotype-matched (IgG1) mouse mAb, MOPC-31C (Sigma), served as a control.

Antibody Labeling

The 11-1F4 antibody (100 μg–1 mg) was labeled with 37–74 MBq of reductant-free ^{125}I (PerkinElmer) or ^{124}I (kindly provided by Dr. George Kabalka, University of Tennessee, Knoxville, TN, and Dr. Ron D. Finn, Memorial Sloan-Kettering Cancer Center, New York, NY, or purchased from IBA/Eastern Isotopes) by use of limiting amounts of *N*-chloro-p-toluenesulfonamide sodium salt (Chloramine-T; Sigma) (*13*). The labeled reagents were suspended in phosphate-buffered saline (PBS) containing bovine serum albumin (BSA) at 5 mg/mL (BSA/PBS), and unbound isotope and protein aggregates were removed by size-exclusion liquid chromatography (*14*) through an Ultrogel AcA34 column (Amersham Pharmacia). Fractions containing IgG monomers were pooled for biodistribution and imaging experiments. ^{125}I-Labeled preparations were subjected to sodium dodecyl sulfate–polyacrylamide gel electrophoresis (SDS-PAGE) (10% gels) in the presence or absence of a reducing agent and analyzed with a Cyclone PhosphorImager (Packard Instrument Co.).

Immunoreactivity Assays

To verify the specificity and affinity of mAb 11-1F4, the radiolabeled antibody was tested in a 96-well plate radioimmunoassay, as well as a bead-conjugated antigen-binding assay. For the former, Immulon 4 (Dynex Technologies) wells were coated with synthetic AL fibrils (and, as a control, nonfibrillar protein). After overnight incubation at 37°C, the wells were incubated with 200 μL of BSA/PBS for 2 h before the addition of 50 μL of serially diluted radiolabeled antibody. The plates were maintained at room temperature on a 60° slanted, rotating disk for 2 h, after which the wells were washed initially with PBS containing 0.1% (v/v) Tween 20 and then with PBS alone. Radioactivity was measured with a Packard COBRA Quantum Gamma Spectrometer (GMI Inc.).

For the bead assay, a 1-mL volume of 0.9-μm-diameter amino-functionalized polystyrene beads (Spherotech Inc.) was washed with PBS and activated by the addition of 4.0 mL of 0.5% glutaraldehyde in PBS for 5 min at room temperature. After another PBS wash, a 1 mg/mL solution of the synthetic Len 1–30 peptide that contained the epitope recognized by mAb 11-1F4 was added to the beads, and the slurry was tumbled end over end for 18 h at room temperature. Free glutaraldehyde sites were then blocked with 0.5 mL of sterile glycine (1 mol/L) in PBS, and the mixture was tumbled for 1 h. After another wash, the beads were stored as a 1:1 slurry in PBS. For the binding assay, 1–10 ng of the radioiodinated antibody was added to 5 μL of the bead suspension in 100 μL of BSA/PBS. After 1 h of incubation, the beads were washed twice with PBS by centrifugation at 10,000*g* for 2 min, and radioactivity was measured with the Gamma Spectrometer.

In Vivo Studies

Amyloidomas were induced in 8-wk-old BALB/c mice by 50-mg subcutaneous injections between the scapulae of human AL fibrils (*5*). After 7 d, the animals received in the lateral tail vein 100- to 200-μL volumes containing 20–50 μg of radiolabeled 11-1F4 or MOPC-31C (~12 MBq) in BSA/PBS. In some studies, a 1% KI (Lugol's) solution was added to the animals' drinking water 48 h before injection to limit radioiodine uptake by the thyroid gland. Mice were euthanized 72 h later by inhalation of an excess of isoflurane, and imaging data were collected. To determine the biodistribution of ^{125}I-labeled antibodies, samples of skin, skeletal muscle, femur, abdominal fat, stomach, small and large intestines, liver, kidneys, spleen, sternum, throat (containing the thyroid), heart, lungs, blood, and brain were harvested, placed into tared vials and weighed, and the radioactivity was measured. The data were expressed as percentage injected dose per gram of tissue (%ID/g). Additionally, samples (including the amyloidomas) were fixed in 10% buffered formalin for 24 h and embedded in paraffin for histologic and autoradiographic analyses.

Single-animal in vivo whole-body clearance measurements were obtained in BALB/c mice injected with 10 μg (5 MBq) of ^{124}I-11-1F4. An unanesthetized mouse was placed at various time intervals into a plastic chamber and lowered into a commercial PET dose calibrator (CRC-15 PET; Capintec) that had been calibrated with known reference standards. Multiple readings were acquired over a 66-h period, and the data were analyzed with mono- or biexponential kinetics. For both forms of radioiodinated mAb 11-1F4, the effective half-life ($T_{½eff}$) was calculated from the measured biologic half-life ($T_{½bio}$) of 11-1F4 and the known physical half-lives ($T_{½rad}$) of ^{124}I and ^{125}I as follows:

$$T_{½eff} = \frac{T_{½bio}T_{½rad}}{T_{½bio} + T_{½rad}}.$$

For autoradiography, 6-μm-thick sections cut from formalin-fixed, paraffin-embedded blocks were placed on Probond microscope slides (Fisher Scientific), dipped in NTB-2 emulsion (Eastman Kodak), stored in the dark, and developed after a 24-h exposure. The sections were counterstained with hematoxylin and eosin or Congo red, placed on coverslips sealed with Permount (Fisher Scientific), and examined by light or polarizing microscopy, respectively. Digital camera microscopic images were obtained and evaluated with an image analysis software package (Image-Pro Plus; Media Cybernetics).

Instrumentation and Image Acquisition

SPECT data were collected with a small-animal SPECT imaging system (developed at the Oak Ridge National Laboratory) (*15*) capable of a 1.7-mm spatial resolution when equipped with a 10-mm-long hexagonal parallel-hole collimator. During imaging,

the 2 detectors [composed of a 50-mm-diameter Hamamatsu R2486-02 multianode photomultiplier tube coupled to a 1 × 1 × 8 mm NaI(Tl) crystal array arranged on a 1.2-mm^2 grid] were positioned ~5 cm from the 50-mL conical tubes housing the mice. Each SPECT dataset comprised 60 projections collected over 360° over the course of 30–60 min. Images were reconstructed with an implementation of the expectation-maximization maximum-likelihood algorithm (*16*).

After the collection of SPECT data, high-resolution CT images were obtained with a MicroCAT II (Siemens Medical Solutions Molecular Imaging, LLC) instrument (*17–19*) with a source and detector configuration capable of an ~75-μm spatial resolution. The scanner had a circular-orbit cone-beam geometry, was equipped with a 20- to 80-kVp microfocus x-ray source, and captured a 90 × 60 mm field of view with a 2,048 × 3,072 charge-coupled device array detector optically coupled to a minR phosphor screen (Eastman Kodak) via a fiber-optic bundle. Each CT dataset, composed of 360 projections at 1° azimuths, was acquired in 8 min. Postacquisition images were reconstructed on isotropic 100-μm voxels by means of a recently developed modified version of the Feldkamp algorithm (*20*). For contrast-enhanced small-animal CT, amyloidoma-bearing mice were given 300-μL intravenous doses of iodinated triglycerides (Fenestra VC; Advanced Research Technologies) 30 min before scanning.

To facilitate coregistration of the reconstructed SPECT and CT images, 3 capillaries filled with a ^{125}I solution and placed on the conical tubes were used for reference purposes and provided fiducial marks in the *x*-, *y*-, and *z*-axes. The small-animal SPECT and CT datasets were visualized and coregistered manually with a 3-dimensional image analysis software package (Amira, version 3.1; Mercury Computer Systems). The volume of each amyloidoma was determined from the small-animal CT data with the Amira tissue segmentation tool.

For PET, euthanized animals were placed on a cardboard platform that contained ^{68}Ge fiducial markers, and data were collected over a 40-min period with the Focus 220 or P4 microPET scanner (Siemens Medical Solutions). The images were reconstructed with the ordered-subset expectation-maximization 3-dimensional maximum *a posteriori* algorithm (*21*). After the collection of small-animal PET data, mice were placed in the MicroCAT II scanner, and the CT dataset was acquired as described earlier. Coregistration of the PET and CT data was performed manually with Amira software.

All animal experiments were conducted in accordance with U.S. Public Health Service guidelines and under the auspices of University of Tennessee and Oak Ridge National Laboratory Animal Care and Use Committee–approved protocols.

RESULTS

Amyloidoma Model

The amyloidomas induced in mice by subcutaneous injections between the scapulae of human AL fibril extracts were readily apparent. After 7 d, the tumors appeared semisolid and vascularized (Fig. 1A), and their size and location were readily documented by small-animal CT (Figs. 1B and 1C). The mean volume of the amyloid lesions, as determined from CT data, was 196 mm^3 (range, 130–260 mm^3).

Radioiodination

The 11-1F4 and MOPC-31C antibodies were readily labeled with ^{125}I and ^{124}I, with yields of up to 80%, depending on the concentration of antibody used in the coupling reaction. PhosphorImager analyses of the radioiodinated proteins after gel filtration and SDS-PAGE indicated that greater than 98% of the radioactivity was localized to the heavy and light chains at a ratio of ~2:1. The dissociation constant (K_d) of radiolabeled 11-1F4 for the Len 1–30 peptide, calculated by Scatchard analysis of radioimmunoassay data, was determined to be ~0.3 nmol/L. When the antibody was tested at a range of 1–10 ng in the bead assay, the maximum binding was 77%–79%. These data demonstrated the purity of radioiodinated mAb 11-1F4 and notably that the affinity of the ^{125}I-11-1F4 conjugate for the Len 1–30 peptide was identical to that of the unlabeled native antibody (*22*).

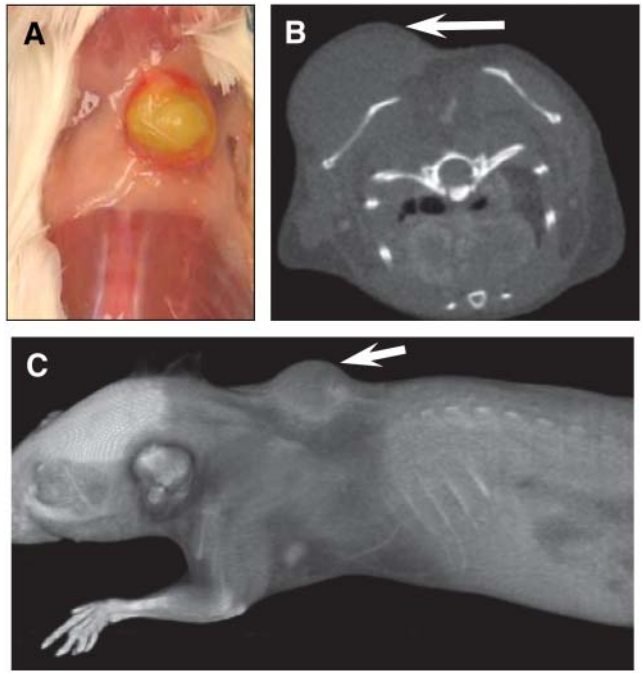

FIGURE 1. Murine model of an AL amyloidoma. (A) Gross appearance of vascularized amyloidoma. (B) Axial slice through upper abdomen of mouse 7 d after 50-mg amyloidoma induction and after administration of an intravenous dose of contrast medium 30 min before image acquisition. (C) Three-dimensional volumetric rendering. Arrows indicate location of amyloidoma. Tumor volume was calculated from small-animal CT data to be 104 mm^3.

Pharmacokinetics of Radiolabeled mAb 11-1F4

Two independent (but complementary) methods were used to determine the pharmacokinetics of mAb 11-1F4. The first method measured the clearance of 25 μg (~4.0 MBq) of ^{125}I-labeled antibody 1, 4, 24, 72, and 144 h after intravenous injection in cohorts of 6 normal, that is, amyloidoma-free, BALB/c mice. At each time point, 1 group of animals was euthanized, the tissues were harvested and weight normalized, and the decay-corrected specific activities were determined (Table 1). For all samples, the activities decreased by 4 h, with the exception of the tongue and skin, in which they more than doubled between the 1- and

TABLE 1
Biodistribution of ^{125}I-Labeled mAb 11-1F4 in Normal BALB/c Mice

Tissue	Mean ± SD %ID/g at:				
	1 h	4 h	24 h	72 h	144 h
Blood	42.5 ± 6.0	32.6 ± 2.2	26.8 ± 1.0	18.4 ± 2.3	16.7 ± 1.0
Skin	1.1 ± 0.3	2.3 ± 0.3	3.1 ± 0.3	2.6 ± 0.2	2.1 ± 0.2
Muscle	1.3 ± 0.2	2.4 ± 0.9	2.1 ± 0.2	1.7 ± 0.3	1.4 ± 0.1
Femur	2.4 ± 0.2	3.0 ± 0.6	2.8 ± 2.2	2.2 ± 0.5	1.9 ± 0.3
Fat pad	0.8 ± 0.1	2.5 ± 0.7	1.9 ± 1.3	1.3 ± 0.2	1.5 ± 0.2
Liver	14.0 ± 0.3	11.4 ± 0.7	8.6 ± 5.7	5.7 ± 1.0	5.6 ± 0.5
Spleen	11.7 ± 1.2	10.0 ± 1.1	8.1 ± 0.6	5.2 ± 0.9	4.6 ± 0.7
Pancreas	2.4 ± 0.5	2.8 ± 0.5	2.7 ± 0.4	1.9 ± 0.2	1.7 ± 0.3
Stomach	2.5 ± 0.4	4.0 ± 0.4	3.1 ± 0.3	2.2 ± 0.1	1.7 ± 0.2
Small intestine	4.1 ± 0.5	4.5 ± 0.5	3.2 ± 0.2	2.4 ± 0.3	2.1 ± 0.2
Cecum	2.5 ± 0.5	5.9 ± 0.4	4.3 ± 0.6	3.0 ± 0.4	2.2 ± 0.3
Large intestine	2.2 ± 0.3	4.1 ± 0.5	3.6 ± 0.2	2.5 ± 0.4	1.9 ± 0.2
Kidney (L)	7.8 ± 1.1	7.8 ± 1.9	5.4 ± 0.6	4.1 ± 0.8	3.4 ± 0.6
Kidney (R)	8.0 ± 1.2	8.2 ± 1.4	5.7 ± 0.7	4.3 ± 0.7	3.4 ± 0.5
Throat*	4.8 ± 1.2	9.0 ± 2.0	6.4 ± 1.6	4.5 ± 0.7	4.3 ± 0.9
Heart	12.6 ± 2.4	10.1 ± 1.4	9.5 ± 2.1	6.4 ± 1.5	5.4 ± 0.6
Lungs	13.8 ± 1.4	13.3 ± 1.9	10.5 ± 0.7	7.2 ± 3.4	6.8 ± 0.6
Tongue	3.4 ± 1.3	8.0 ± 0.9	7.2 ± 0.7	8.8 ± 7.7	4.4 ± 0.4
Brain	0.9 ± 0.2	0.8 ± 0.1	0.6 ± 0.1	0.5 ± 0.1	0.4 ± 0.1

*Tissue includes esophagus and thyroid gland (n = 6).

4-h collection times and remained at ~8 and 2.6 %ID/g, respectively, for up to 72 h after injection. However, at the 144-h time point, the activities in both sites declined. At 1 h after injection, ~42% of the dose remained in the circulation; the plasma clearance rate, calculated from the measured activity in blood samples corrected for isotope decay, was described by biexponential decay (Fig. 2A), with $T_{½bio}$ values of 1.9 ± 1.3 (mean ± SD) and 164.1 ± 67.8 h (R^2 = 0.98) for the α- and β-components of exponential decay, respectively.

The second method measured the whole-body clearance of 10 μg of ^{124}I-11-1F4 (~4.5 MBq) in unanesthetized mice (n = 3). The decay-corrected rate of disappearance of the radioiodinated antibody over a 72-h period fit equivalently to both biexponential and monoexponential curves (R^2 = 0.91) (Fig. 2B); however, only the latter provided a realistic value (177.7 ± 19.8 h) for $T_{½bio}$. These data compare favorably with those for the β-component of exponential decay calculated from the plasma clearance rate as well as with the $T_{½bio}$ for murine IgG1 in mice (*23–25*). Using $T_{½rad}$ values of 100 h for ^{124}I and 1,426 h for ^{125}I, we found the $T_{½eff}$ values for ^{124}I-labeled and ^{125}I-labeled mAb 11-1F4 to be 64 and 158 h, respectively.

Biodistribution of Radioiodinated mAb 11-1F4

The in vivo behaviors of the ^{125}I-labeled fibril-reactive 11-1F4 and control MOPC-31C antibodies were studied in mice bearing amyloidomas composed of human ALκ or ALλ fibrils. The time chosen for injection of the radiolabeled reagents (7 d after induction) resulted from our finding that these tumors remained unchanged in size during this period and, as shown in Figure 1A, also had become vascularized. In studies in which cohorts of amyloidoma-bearing mice received 25 μg (~4 MBq) of ^{125}I-11-1F4 and were euthanized 1, 24, 72, and 100 h later, a comparison of radioactivity in tumors against that found in body organs or tissues revealed no significant divergence 1 and 24 h after injection because of the high blood-pool background; however, at 72 h, there was selective uptake by the amyloidomas. Thus, the biodistribution (and subsequent imaging) experiments were performed 72 h after antibody injection. The results of studies in which mice bearing different ALκ amyloidomas were injected with 10 μg (~11 MBq) of ^{125}I-11-1F4 are shown in Figure 3A. The recovery of ^{125}I in the harvested amyloidomas ranged from 12 to 43 %ID/g, with a mean of 22 %ID/g, a value significantly higher than that seen in skeletal muscle (1.2 %ID/g) ($P < 0.001$), spleen (3.9 %ID/g) ($P < 0.001$), kidney (4.8 %ID/g) ($P < 0.01$), heart (5.0 %ID/g) ($P < 0.01$), and liver (5.8 %ID/g) ($P > 0.05$), as well as other tissues examined. This reagent also was taken up selectively, albeit to a lesser extent, by ALλ tumors (n = 5); the specific activities ranged from 6 to 12 %ID/g, with a mean of 9.5 %ID/g (Fig. 3B). The amyloid-to-liver ratios for ALκ and ALλ amyloidomas were ~3.8:1 and 2.3:1, respectively. In contrast, this ratio was 1.1:1 for the radiolabeled control MOPC-31C antibody, indicating that there was essentially no binding to the amyloidoma.

Autoradiography

At 7 d after amyloidoma induction, mice were injected with ~11 MBq of ^{125}I-11-1F4 or ^{125}I-MOPC-31C antibody. The former reagent localized to the amyloid mass, as evidenced in autoradiograms by the deposition of the γ-emitting

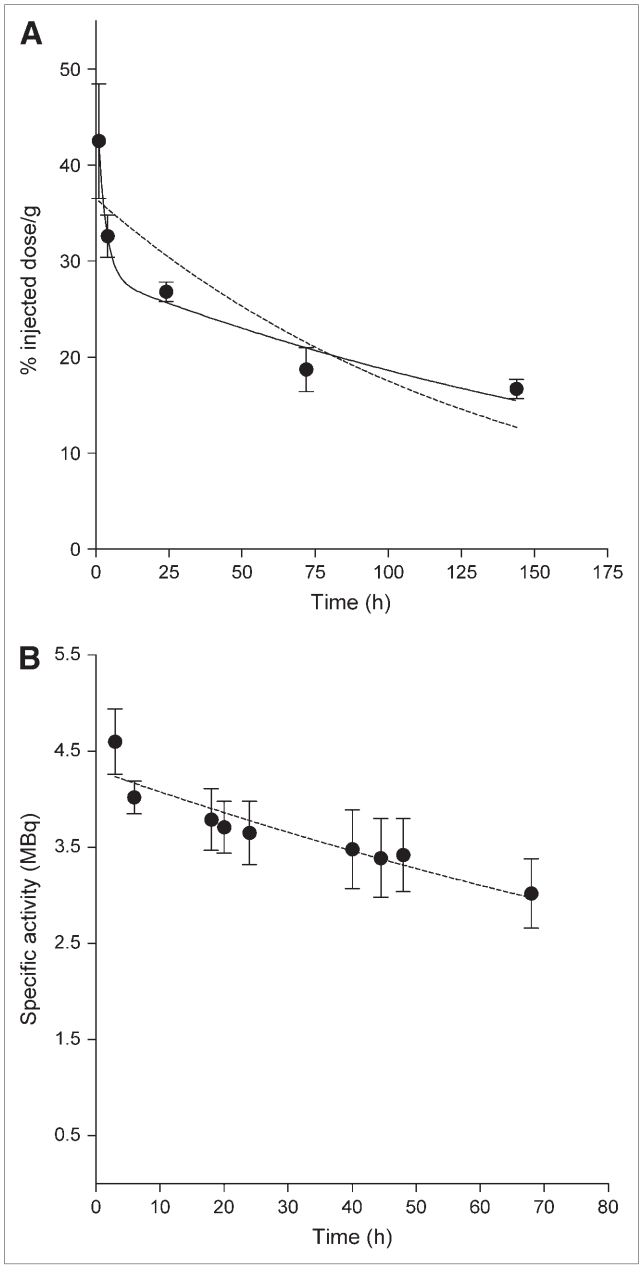

FIGURE 2. Pharmacokinetics of radioiodinated mAb 11-1F4. Plasma (A) and whole-body (B) clearance kinetics for ^{125}I- and ^{124}I-labeled mAb 11-1F4, respectively, injected into normal mice (6 and 3 animals at each time point for ^{125}I and ^{124}I studies, respectively). Mono- and biexponential fits to data are represented by dashed and solid lines, respectively. No convergence was achieved with biexponential equation for data in B.

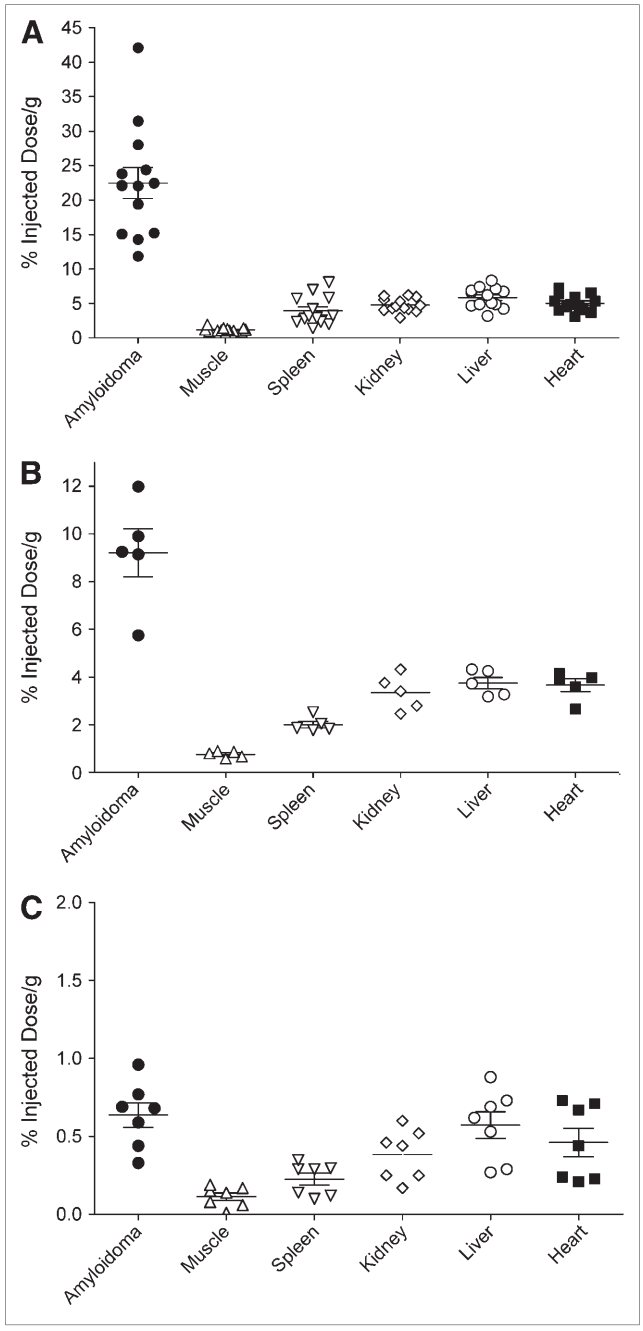

FIGURE 3. Biodistribution of radiolabeled mAb 11-1F4. (A and B) Comparison of amyloidoma vs. tissue uptake 72 h after injection of ^{125}I-11-1F4 in mice bearing ALκ (A) or ALλ (B) amyloidomas. (C) Data for ^{125}I-MOPC-31C (control antibody) given to mice with ALκ amyloidomas. Bars indicate mean ± SD. Note different scales on ordinates.

isotope within the green birefringent congophilic material (Fig. 4). Consistent with the biodistribution data, there was more uptake of mAb 11-1F4 by ALκ amyloidomas than by ALλ amyloidomas. Examination of other tissues revealed small deposits in sites associated with the blood pool, such as hepatic sinusoids, heart ventricles, and renal tubules. In contrast, there was essentially no detectable binding in experiments involving the radiolabeled control antibody.

Small-Animal SPECT/CT

In small-animal SPECT/CT studies of mice bearing 50-mg amyloidomas that received a 200-μL dose containing 50 μg of ^{125}I-11-1F4 (~11 MBq), the images acquired 72 h after injection revealed that the most intense region of radioactivity occurred dorsally and corresponded exactly to the location of the amyloidomas, as visualized by CT (Fig. 5A).

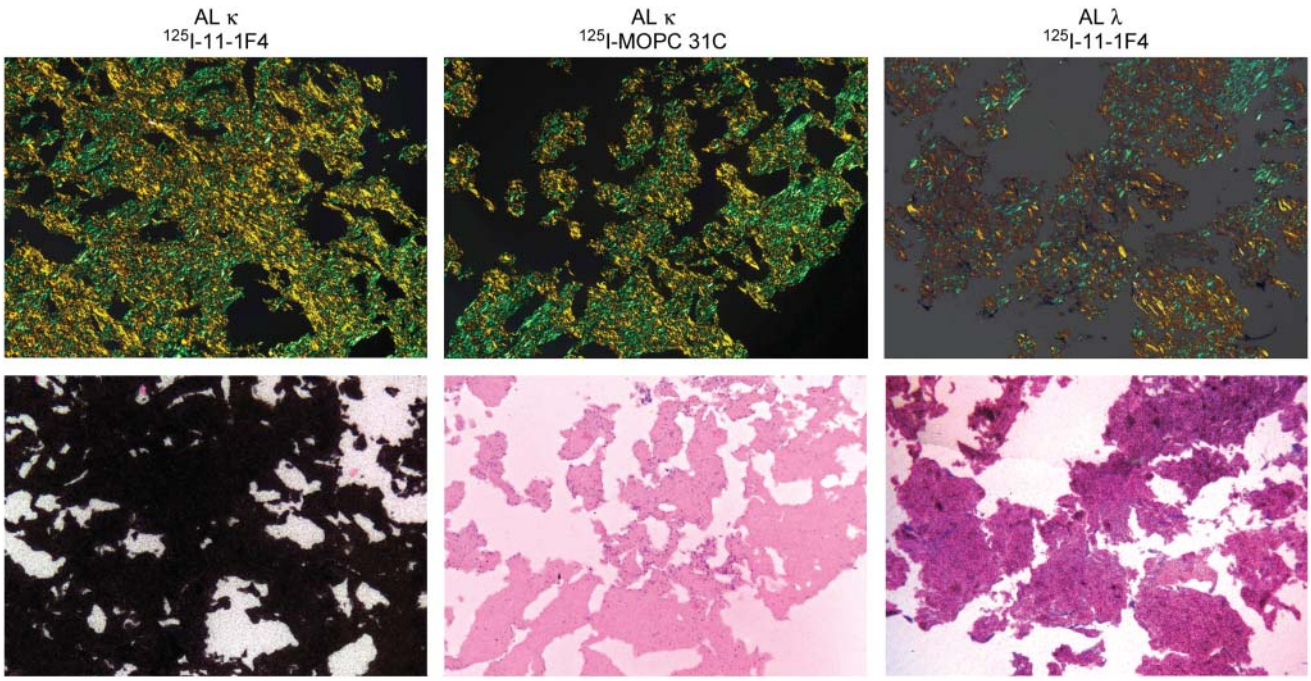

FIGURE 4. Autoradiographic localization within human AL amyloidomas of radioiodinated mAb 11-1F4. ALκ and ALλ amyloidoma–bearing mice were injected 7 d after induction with either ^{125}I-labeled fibril-reactive (11-1F4) or control (MOPC-31C) antibody, and tumors were harvested 72 h later. (Top row) Congo red–stained sections (polarizing microscopy; original magnification, ×80). (Bottom row) Microautoradiographs (exposure, 72 h; original magnification, ×80). %ID/g values for ^{125}I-11-1F4 in ALκ and ALλ tumors were 43 and 9, respectively.

There also was modest uptake of the isotope by the liver, tongue, and thyroid, as evidenced in the surface plot of a sagittal plane passing through the center of the mouse (Fig. 5B). The SPECT signal from these non–amyloid-containing tissues was considered background activity associated with the uptake of free iodide, which could be excluded when a threshold value of 60% maximum was implemented (Figs. 5F–5H). Under these conditions, only ALλ and ALκ amyloidomas were readily visualized (Figs. 5F and 5G). In all cases, there was no visible deposition of the radiolabeled control MOPC-31C antibody (Figs. 5C, 5D, and 5H).

Small-Animal PET/CT Imaging

Given that ^{125}I is unsuitable for clinical imaging purposes, we used the positron-emitting isotope ^{124}I to label mAb 11-1F4. AL amyloidoma-bearing mice were injected with ~4 MBq of the radioiodinated antibody and euthanized 72 h later (whole-body images were acquired postmortem to prevent the loss of resolution attributable to cardiac and respiratory motion artifacts). The results of such a study are shown in Figure 6. The small-animal PET image indicated that the radioactivity was confined principally to a dorsal area corresponding anatomically to the location of the amyloidomas, with negligible amounts in the blood pool. From the coregistered PET/CT images, ^{124}I-11-1F4 was localized more precisely to the interscapular region. In contrast, in animals that received the control ^{124}I-MOPC-31C antibody, minimal activity was present only in the blood pool (data not shown).

DISCUSSION

We have shown that radioiodinated derivatives of the fibril-reactive mAb 11-1F4 could be used to image amyloid tumors in an experimental in vivo murine model. This antibody was effectively radiolabeled with either ^{125}I or ^{124}I without an adverse effect on its immunoreactivity (as evidenced in 2 independent assays) or pharmacokinetics. Biodistribution studies in which ^{125}I-11-1F4 was given to amyloidoma-bearing animals and the tissues were harvested 72 h later revealed that the radioactivity was concentrated in the amyloid tumors. We attribute the greater accumulation of antibody in ALκ than in ALλ amyloidomas (22 vs. 9 %ID/g) to possible differences in the expression of the conformation-related fibril epitope recognized by mAb 11-1F4 (which also was found to be more effective in accelerating amyloidolysis in mice bearing ALκ tumors than in those bearing ALλ tumors) (*5*). The binding of 11-1F4 to extracted ALκ fibrils was ~3-fold greater than that to ALλ fibrils, as determined by an enzyme-linked immunosorbent assay (Jonathan S. Wall and Alan Solomon, submitted). Nonetheless, the radioiodinated reagent accumulated in ALλ (as well as ALκ) amyloidomas in amounts sufficient to be visualized by SPECT. Further, through the use of high-resolution dual-modality imaging technology, it was possible to localize precisely the isotope specifically within the amyloidomas; in addition, autoradiograms of the amyloid tumors showed a nearly uniform distribution of the radioisotope throughout the mass, indicating efficient perfusion of the amyloidomas from the established vasculature.

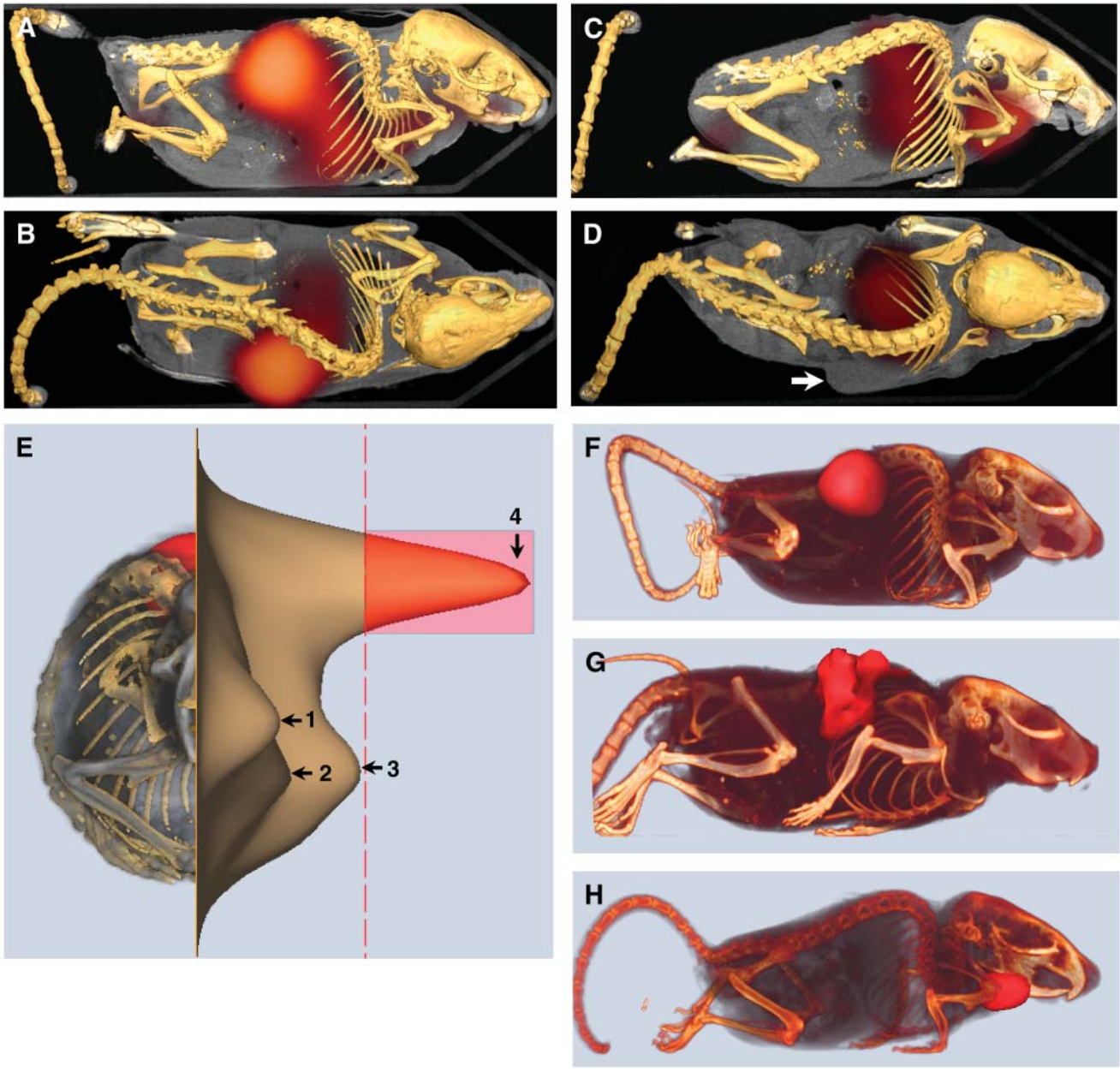

FIGURE 5. Radioimaging of human AL amyloidomas by small-animal SPECT/CT. Amyloid-bearing mice were injected with ^{125}I-11-1F4 antibody (A, B, E, F, and G) or control MOPC-31C antibody (C, D, and H) and scanned 72 h later. (A and C) Left lateral SPECT/CT images of ^{125}I-11-1F4 and ^{125}I-MOPC-31C, respectively, in ALκ amyloidoma–bearing mouse (threshold for SPECT, 10% maximum value). (B and D) Dorsal–ventral SPECT/CT images of ^{125}I-11-1F4 and ^{125}I-MOPC-31C, respectively, in ALκ amyloidoma–bearing mouse (threshold for SPECT, 10% maximum value; arrow indicates amyloidoma visible in CT image only). (E) Intensity of ^{125}I activity along sagittal plane bisecting amyloidoma (line and shaded area coincide with 60% maximum-intensity threshold for SPECT applied to F, G, and H; 1, 2, 3, and 4 indicate tongue, thyroid, liver, and amyloidoma, respectively). (F and G) Representative images of ^{125}I-11-1F4–injected mice bearing ALκ (F) and ALλ (G) amyloidomas; thresholded SPECT is shown as isosurface. (H) Image of mouse with induced ALκ amyloidoma that received control ^{125}I-MOPC-31C antibody (isosurface rendering). Volumes of amyloidomas in mice shown in A, B, and F; in C, D, and H; in E; and in G were 260, 130, 120, and 196 mm^3, respectively.

Notably, the significantly higher %ID/g of mAb 11-1F4 in amyloid than in various organs indicates the potential of this reagent to image pathologic deposits in patients with systemic AL amyloidosis.

Although ^{125}I-labeled 11-1F4 proved suitable for the small-animal SPECT studies in mice because of their modest axial diameter and the subcutaneous location of the amyloid-containing masses, the low γ-energy of this nuclide precludes its use in humans. Additionally, given the fact that the optimum time for imaging with this mAb is 72 h after injection, the short half-lives of ^{123}I and ^{99m}Tc, as well as the limited resolution that can be achieved with

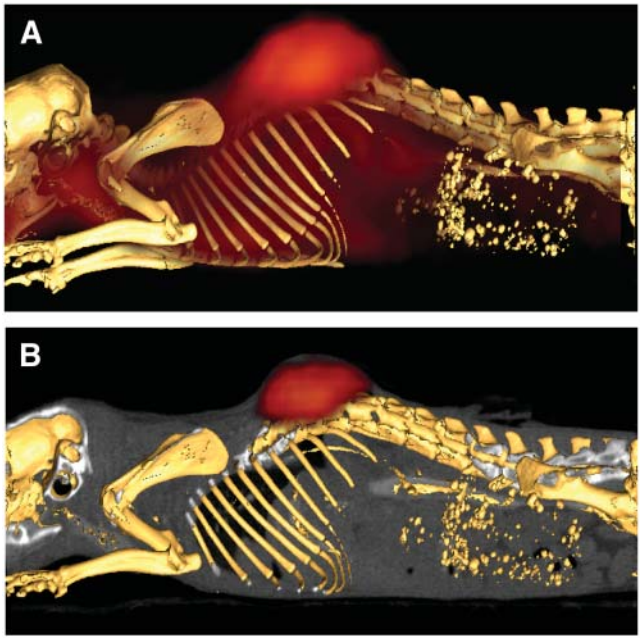

FIGURE 6. Radioimaging of human amyloid by small-animal PET/CT. Volume-rendered, coregistered PET/CT images are shown for an AL amyloidoma–bearing mouse injected with ^{124}I-11-1F4 and scanned 72 h later. (A) Coregistered small-animal CT and small-animal PET (threshold of 10% maximum intensity for PET). (B) Small-animal PET/CT image (PET data threshold at ≥60% maximum intensity).

^{111}In, also would render these isotopes unsuitable. Although the optimum scan time could be shortened with the use of the $F(ab')_2$ mAb fragment, the short biologic half-life resulted in decreased accumulation of the molecule in the amyloidomas and inferior images (data not shown). Because radioiodination with ^{125}I did not adversely affect the amyloid-binding properties of mAb 11-1F4, we chose to use another iodine nuclide with the requisite half-life (4 d), namely, the positron-emitting isotope ^{124}I. Further, the higher sensitivity and ability to collect quantitative data (*26–28*) make PET more desirable than SPECT as a potential amyloid imaging modality. When mice were given ^{124}I-11-1F4, this reagent was taken up selectively by the human AL amyloidomas with minimal background radioactivity. Indeed, the feasibility of immunoimaging by PET has been evidenced in studies involving ^{124}I-labeled antibodies for colorectal cancer (*29*), HER 2/neu (*26*), and carcinoembryonic antigen (*30*). In the latter 2 cases, the tracers contained genetically engineered antibody fragments, that is, minibodies and diabodies; because these fragments had lower molecular masses than the intact molecule, they had considerably faster blood clearance and tumor uptake. In this regard, our future studies will involve preparing modified derivatives of mAb 11-1F4 and testing their effectiveness as imaging agents for patients with AL amyloidosis and other forms of systemic amyloidosis.

CONCLUSION

Heretofore, clinicians have had only limited means to ascertain the amyloid burden in patients with AL amyloidosis and other systemic amyloidoses. The availability of a radiolabeled fibril-reactive mAb that can be used to document objectively the presence and amount of amyloid in such individuals should provide a novel and much needed diagnostic tool for the management of these disorders. The biodistribution and coregistered SPECT/CT and PET/CT data, which indicated selective uptake of radiolabeled mAb 11-1F4 by the human AL amyloidomas with a favorable signal-to-noise ratio, indicate the feasibility of using this reagent to image amyloid. The experimental results obtained with the ^{124}I-labeled antibody validate testing this technology in a clinical trial.

ACKNOWLEDGMENTS

The technical assistance of Dr. Rudi Hrncic, Dr. Shaun Gleason, Dr. Justin Baba, Dennis A. Wolfenbarger, Teresa K. Williams, Trish Lankford, Sallie D. Macy, Craig Wooliver, and James Wesley and manuscript preparation by Alisa Lehberger are gratefully acknowledged. This work was supported, in part, by NIBIB/NINDS Bioengineering Research Partnership Award EB00789; USPHS Research Grant CA-10056 from the National Cancer Institute; Amgen, Inc.; and the Aslan Foundation.

REFERENCES

1. Aprile C, Marinone G, Saponaro R, Bonino C, Merlini G. Cardiac and pleuropulmonary AL amyloid imaging with technetium-99m labelled aprotinin. *Eur J Nucl Med.* 1995;22:1393–1401.
2. Hachulla E, Maulin L, Deveaux M, et al. Prospective and serial study of primary amyloidosis with serum amyloid P component scintigraphy: from diagnosis to prognosis. *Am J Med.* 1996;101:77–87.
3. Hawkins PN, Lavender JP, Pepys MB. Evaluation of systemic amyloidosis by scintigraphy with ^{123}I-labeled serum amyloid P component. *N Engl J Med.* 1990; 323:508–513.
4. Schaadt BK, Hendel HW, Gimsing P, Jonsson V, Pedersen H, Hesse B. ^{99m}Tc-Aprotinin scintigraphy in amyloidosis. *J Nucl Med.* 2003;44:177–183.
5. Hrncic R, Wall J, Wolfenbarger DA, et al. Antibody-mediated resolution of light chain-associated amyloid deposits. *Am J Pathol.* 2000;157:1239–1246.
6. Pras M, Schubert M, Zucker-Franklin D, Rimon A, Franklin EC. The characterization of soluble amyloid prepared in water. *J Clin Invest.* 1968;47: 924–933.
7. Murphy CL, Eulitz M, Hrncic R, et al. Chemical typing of amyloid protein contained in formalin-fixed paraffin-embedded biopsy specimens. *Am J Clin Pathol.* 2001;116:135–142.
8. Wall J, Schell M, Murphy C, Hrncic R, Stevens FJ, Solomon A. Thermodynamic instability of human lambda 6 light chains: correlation with fibrillogenicity. *Biochemistry.* 1999;38:14101–14108.
9. Schneider M, Hilschmann N. The primary structure of a monoclonal immunoglobulin L-chain of kappa-type, subgroup IV (Bence-Jones protein Len): a new subgroup of the kappa-type L-chain. *J Physiol Chem.* 1974;355:1164–1168.
10. Abe M, Goto T, Wolfenbarger D, Weiss DT, Solomon A. Novel immunization protocol and ELISA screening methods used to obtain and characterize monoclonal antibodies specific for human light chain variable-region subgroups. *Hybridoma.* 1993;12:475–483.
11. Solomon A, Weiss DT, Wall JS. Therapeutic potential of chimeric amyloid-reactive monoclonal antibody 11-1F4. *Clin Cancer Res.* 2003;9(suppl):3831S–3838S.
12. Solomon A, Weiss DT, Wall JS. Immunotherapy in systemic primary (AL) amyloidosis using amyloid-reactive monoclonal antibodies. *Cancer Biother Radiopharm.* 2003;18:853–860.
13. Kennel SJ, Foote LJ, Lankford PK, Johnson M, Mitchell T, Braslawsky GB. Direct binding of radioiodinated monoclonal antibody to tumor cells: significance of antibody purity and affinity for drug targeting or tumor imaging. *Hybridoma.* 1983;2:297–309.

14. Kennel SJ, Lankford TK, Foote LJ, Shinpock SG, Stringer C. CD44 expression on murine tissues. *J Cell Sci.* 1993;104:373–382.
15. Wall JS, Kennel SJ, Paulus MJ, et al. Quantitative high-resolution microradiographic imaging of amyloid deposits in a novel murine model of AA amyloidosis. *Amyloid.* 2005;12:149–156.
16. Shepp LA, Vardi Y. Maximum-likelihood reconstruction for emission tomography. *IEEE Trans Med Imaging.* 1982;1:113–122.
17. Paulus M, Gleason SS, Kennel SJ, Hunsicker PR, Johnson DK. High resolution X-ray computed tomography: an emerging tool for small animal cancer research. *Neoplasia.* 2000;2:62–70.
18. Paulus MJ, Gleason SS, Sari-Sarraf H, et al. High-resolution x-ray CT screening of mutant mouse models. In: Farkas DL, Leif RC, eds. *BIOS 2000 International Biomedical Optics Symposium*. San Jose, CA: *SPIE-Int. Soc. Opt. Eng.*; 2000: 270–279.
19. Paulus MJ, Sari-Sarraf H, Gleason SS, et al. A new x-ray computed tomography system for laboratory mouse imaging. *IEEE Trans Nucl Sci.* 1999;46:558–564.
20. Gregor J, Gleason SS, Paulus MJ, Cates J. Fast Feldkamp reconstruction based on focus of attention and distributed computing. *Int J Imag Syst Tech.* 2002; 12:229–234.
21. Qi J, Leahy RM. Resolution and noise properties of MAP reconstruction for fully 3-D PET. *IEEE Trans Med Imaging.* 2000;19:493–506.
22. O'Nuallain B, Murphy CL, Wolfenbarger DA, Kennel S, Solomon A, Wall JS. The amyloid-reactive monoclonal antibody 11-1F4 binds a cryptic epitope on fibrils and partially denatured immunoglobulin light chains and inhibits fibrillogenesis. In: Grateau G, Kyle RA, Skinner M, eds. *Xth International Symposium on Amyloidosis*. Tours, France: CRC Press; 2005:482-484.
23. Gurbaxani B, Dela Cruz LL, Chintalacharuvu K, Morrison SL. Analysis of a family of antibodies with different half-lives in mice fails to find a correlation between affinity for FcRn and serum half-life. *Mol Immunol.* 2006;43:1462–1473.
24. Levy AL, Waldmann TA. The effect of hydrocortisone on immunoglobulin metabolism. *J Clin Invest.* 1970;49:1679–1684.
25. Montano RF, Morrison SL. Influence of the isotype of the light chain on the properties of IgG. *J Immunol.* 2002;168:224–231.
26. Gonzalez Trotter DE, Manjeshwar RM, Doss M, et al. Quantitation of small-animal ^{124}I activity distributions using a clinical PET/CT scanner. *J Nucl Med.* 2004;45:1237–1244.
27. Herzog H, Tellman L, Qaim SM, Spellerberg S, Schmid A, Coenen HH. PET quantitation and imaging of the non-pure positron-emitting iodine isotope ^{124}I. *Appl Radiat Isot.* 2002;56:673–679.
28. Pentlow KS, Graham MC, Lambrecht RM, et al. Quantitative imaging of iodine-124 with PET. *J Nucl Med.* 1996;37:1557–1562.
29. Lee FT, Hall C, Rigopoulos A, et al. Immuno-PET of human colon xenograft–bearing BALB/c nude mice using ^{124}I-CDR-grafted humanized A33 monoclonal antibody. *J Nucl Med.* 2001;42:764–769.
30. Sundaresan G, Yazaki PJ, Shively JE, et al. ^{124}I-Labeled engineered anti-CEA minibodies and diabodies allow high-contrast, antigen-specific small-animal PET imaging of xenografts in athymic mice. *J Nucl Med.* 2003;44:1962–1969.